Steel and Composite Structures, *Vol. 22, No. 5 (2016) 1073-1084*
DOI: http://dx.doi.org/10.12989/scs.2016.22.5.1073

Study on rectangular concrete-filled steel tubes with unequal wall thickness

Yang Zhang [1,2], Chen-Jiang Yu [1], Guang-Yuan Fu [1],
Bing Chen [3], She-Xu Zhao [1] and Si-Ping Li [*1]

[1] *Department of Engineering Mechanics, Shanghai Jiao Tong University, Shanghai 200240, P.R. China*
[2] *School of Civil Engineering, Nanyang Institute of Technology, Nanyang 473004, P.R. China*
[3] *Department of Civil Engineering, Shanghai Jiao Tong University, Shanghai 200240, P.R. China*

(*Received September 21, 2015, Revised October 26, 2016, Accepted November 11, 2016*)

Abstract. Rectangular concrete-filled steel tubular columns with unequal wall thickness were investigated in the paper. The physical centroid, the centroidal principal axes of inertia, and the section core were given. The generalized bending formula and the generalized eccentric compression formula were deduced, and the equation of the neutral axis was also provided. The two rectangular concrete-filled steel tubular stub specimens subjected to the compression load on the physical centroid and the geometric centroid respectively were tested to verify the theoretical formulas.

Keywords: CFST; asymmetric cross section; physical centroid; generalized bending formula; generalized eccentric compression formula; cross section core

1. Introduction

Concrete-filled steel tubular (CFST) columns have been widely used in the constructions nowadays, which have a lot of advantages, such as high load capacity, high ductility, and large energy-absorption capacity (Han 2002, Xiao *et al*. 2012, Abdalla *et al*. 2013, Ren *et al*. 2014a, b, Uenaka 2014, Hou *et al*. 2013). There are many types of cross sections of CFST columns, such as circle, square, rectangle, and octagon. Square and rectangular CFST columns are easier to construct nodes, and have better bending performance than others. In general, the wall thickness of steel tubes is uniform, which is beneficial to the processing of steel tubes.

Research into CFST columns has been carried out throughout the world for many years, and a lot of research achievements have been obtained (Giakoumelis and Lam 2004, Gupta *et al*. 2007, Jiang *et al*. 2010, Chen *et al*. 2011, Chung *et al*. 2013, Dai and Lam 2010, Kvedaras *et al*. 2015). Abed *et al*. (2013) experimentally investigated the effect of diameter-to-thickness ratio, and concrete compressive strength on the bearing capacity of circular CFST columns under axial compression. They concluded that diameter-to-thickness ratio was the main factor on the compressive performance of circular CFST columns. Evirgen *et al*. (2014) experimentally studied CFST columns subjected to axial loading and focused on the effect of width-to-thickness ratio, concrete compressive strength and cross-sectional shape on the ultimate capacity, axial stress,

*Corresponding author, Professor, E-mail: lisp_sjtu@sina.com

 ISSN: 1229-9367 (Print), 1598-6233 (Online)

ductility and buckling behavior. Four cross-sectional shapes of circle, hexagon, rectangle and square, four width-to-thickness ratios ranging between 18.75 and 100.00 and three concrete compressive strengths of 13, 26 and 35 MPa were investigated. The results showed that circular cross-section was most effective according to both axial stress and ductility.

However, the existing studies mainly focus on CFST columns with uniform wall thickness, and there is little research concerning CFST columns with unequal wall thickness. The uniform wall thickness is not conducive to make full use of materials, and the unequal wall thickness is a good choice for the cross section optimization. So it is very necessary to investigate the CFST columns with unequal wall thickness and provide the general formulas which can be degenerated into special cases. The objective of this investigation is fourfold: first, to investigate the section properties of rectangular CFST columns with unequal wall thickness; second, to deduce the generalized bending formula; third, to deduce the generalized eccentric compression formula and determine the cross section core; fourth, to verify these theoretical formulas through experiments.

2. General formulas of rectangular CFST columns with unequal wall thickness

2.1 Physical centroid

The rectangular steel tube is welded with 4 steel plates with different wall thickness t_1, t_2, t_3 and t_4. As shown in Fig. 1, the cross section is with a breadth of B and a height of H. The Young's modulus of different steel plates is assumed to be the same. The coordinate system is located in the geometric centroid (C) of the cross section.

The cross section shown in Fig. 1 is asymmetric, and when the axial load acts on the physical centroid (C_p) of the cross section the whole section will deform uniformly. In the elastic stage, the axial load can be expressed as follows

$$N = E_s A_s \varepsilon + E_c A_c \varepsilon \tag{1}$$

where ε is the axial strain, A_s is the cross-sectional area of the steel hollow section, A_c is the cross-sectional area of the concrete core, E_s is the Young's modulus of steel, and E_c is the Young's modulus of concrete. Based on the theorem of the resultant moment, the physical centroid of the cross section is determined as follows

$$y_{C_p} = k_p e_y, \qquad z_{C_p} = k_p e_z \tag{2}$$

where k_p, e_y and e_z are calculated as below

$$k_p = \frac{m_E - 1}{m_E + \alpha_{sc}}, \qquad e_y = \frac{t_1 - t_2}{2}, \qquad e_z = \frac{t_3 - t_4}{2} \tag{3}$$

where m_E is the Young's modulus ratio, i.e., E_c/E_s, and α_{sc} is the steel ratio, i.e., A_s/A_c.

Based on Eq. (1), the combined Young's modulus (E_{sc}) of CFST specimens can be defined as follows

$$E_{sc} = \frac{E_s A_s + E_c A_c}{A} \tag{4}$$

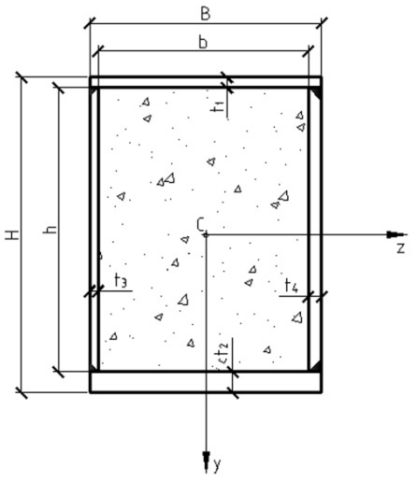

Fig. 1 Cross section of rectangular CFST columns with unequal wall thickness

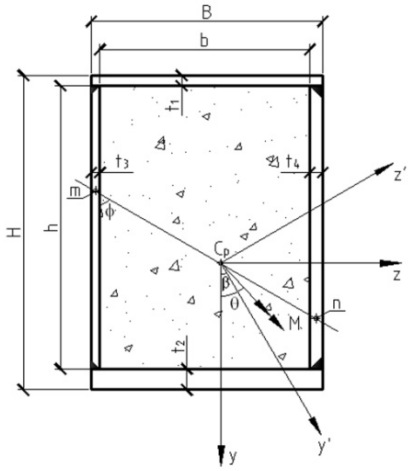

Fig. 2 Cross section of rectangular CFST beams with unequal wall thickness subjected to pure bending

where A is the cross-sectional area of the whole section.

2.2 Generalized bending formula

The rectangular CFST beam with unequal wall thickness is assumed to be subjected to pure bending. As shown in Fig. 2, the coordinate system is located in the physical centroid, and the bending moment of M forms an angle of θ with the y axis. The centroidal principal axes of inertia are assumed to be the axes of y' and z' as shown in Fig. 2, which are obtained by rotating the coordinate system of yz an angle of β around the origin counterclockwise. The transformation relationship between the two sets of the coordinate systems is expressed as below

$$y' = y\cos\beta + z\sin\beta, \qquad z' = -y\sin\beta + z\cos\beta \tag{5}$$

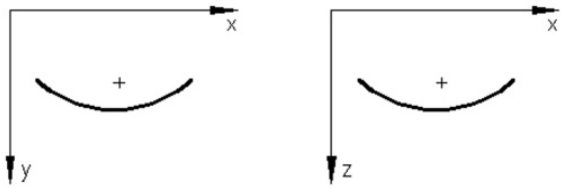

Fig. 3 Positive curvature

The following assumptions are used:

(1) Planar cross section assumption, i.e., the cross section remains plane after deformation.
(2) Tensile stress is assumed to be positive, and compressive stress is assumed to be negative.
(3) Bending moment pointing to the positive direction of the coordinate axis is assumed to be positive; conversely, negative.
(4) Curvature is assumed to be positive if the deflection curve protrudes to the positive direction of the coordinate axis; conversely, negative. The positive curvature is illustrated in Fig. 3.

In the elastic stage, the bending stress of the cross section can be expressed as follows

$$\sigma_s = \kappa_{y'} E_s y' + \kappa_{z'} E_s z', \qquad \sigma_c = \kappa_{y'} E_c y' + \kappa_{z'} E_c z' \tag{6}$$

where σ_s is the bending stress of the steel tube, σ_c is the bending stress of the concrete core, $\kappa_{y'}$ is the curvature of y' direction, and $\kappa_{z'}$ is the curvature of z' direction. The equilibrium equations of the cross section can be established as below

$$\int_{A_s} \sigma_s dA + \int_{A_c} \sigma_c dA = 0 \tag{7}$$

$$\int_{A_s} \sigma_s z dA + \int_{A_c} \sigma_c z dA = M_y \tag{8}$$

$$-\int_{A_s} \sigma_s y dA - \int_{A_c} \sigma_c y dA = M_z \tag{9}$$

where M_y and M_z are the components of the bending moment and calculated as follows

$$M_y = M\cos\theta, \qquad M_z = M\sin\theta \tag{10}$$

The static moments of S_y and S_z, the inertia moments of I_y and I_z, and the inertia product of I_{yz} of the CFST cross section are generally defined as follows

$$S_y = \int_A z dA - (1-m_E)\int_{A_c} z dA, \qquad S_z = \int_A y dA - (1-m_E)\int_{A_c} y dA \tag{11}$$

$$I_y = \int_A z^2 dA - (1-m_E)\int_{A_c} z^2 dA, \qquad I_z = \int_A y^2 dA - (1-m_E)\int_{A_c} y^2 dA \tag{12}$$

$$I_{yz} = \int_A yzdA - (1-m_E)\int_{A_c} yzdA \tag{13}$$

The static moments are equal to zero, which is due to the coordinate axes passing through the physical centroid. The inertia moments and the inertia product of the cross section of the rectangular CFST beam with unequal wall thickness are calculated as below

$$I_y = \frac{HB^3}{12} - (1-m_E)\frac{hb^3}{12} + k_p BHe_z^2, \qquad I_z = \frac{BH^3}{12} - (1-m_E)\frac{bh^3}{12} + k_p BHe_y^2 \tag{14}$$

$$I_{yz} = k_p BHe_y e_z \tag{15}$$

Based on the axial conversion formula, the inertia product of $I_{y'z'}$, which is equal to zero, can be calculated as follows

$$I_{y'z'} = I_{yz}\cos 2\beta + \frac{I_y - I_z}{2}\sin 2\beta \tag{16}$$

The angle of β, which represents the orientation of the centroidal principal axes of inertia, can be determined as below

$$\beta = \frac{1}{2}\arctan(-\frac{2I_{yz}}{I_y - I_z}) \tag{17}$$

By introducing Eqs. (5)-(6) into Eqs. (7)-(9), the following equations are obtained

$$\kappa_{y'}S_{z'} + \kappa_{z'}S_{y'} = 0 \tag{18}$$

$$\kappa_{y'}E_s(I_y \sin\beta + I_{yz}\cos\beta) + \kappa_{z'}E_s(I_y \cos\beta - I_{yz}\sin\beta) = M_y \tag{19}$$

$$-\kappa_{y'}E_s(I_z \cos\beta + I_{yz}\sin\beta) - \kappa_{z'}E_s(-I_z \sin\beta + I_{yz}\cos\beta) = M_z \tag{20}$$

Eq. (18) is naturally satisfied due to the static moments of $S_{y'}$ and $S_{z'}$ being equal to zero. The curvatures of $\kappa_{y'}$ and $\kappa_{z'}$ can be obtained by solving Eqs. (19)-(20) as follows

$$\begin{aligned}
\kappa_{y'} &= \frac{-M_z(I_y \cos\beta - I_{yz}\sin\beta) - M_y(-I_z \sin\beta + I_{yz}\cos\beta)}{E_s(I_y I_z - I_{yz}^2)} \\
\kappa_{z'} &= \frac{M_z(I_y \sin\beta + I_{yz}\cos\beta) + M_y(I_z \cos\beta + I_{yz}\sin\beta)}{E_s(I_y I_z - I_{yz}^2)}
\end{aligned} \tag{21}$$

By introducing the Eqs. (5), (10) and (21) into Eq. (6), the generalized bending formula is obtained and expressed as follows

$$\begin{aligned}\sigma_s &= \frac{(M_y I_z + M_z I_{yz})z - (M_z I_y + M_y I_{yz})y}{I_y I_z - I_{yz}^2} \\ &= \frac{M((I_z \cos\theta + I_{yz}\sin\theta)z - (I_y \sin\theta + I_{yz}\cos\theta)y)}{I_y I_z - I_{yz}^2} \\ \sigma_c &= m_E \frac{(M_y I_z + M_z I_{yz})z - (M_z I_y + M_y I_{yz})y}{I_y I_z - I_{yz}^2} \\ &= m_E \frac{M((I_z \cos\theta + I_{yz}\sin\theta)z - (I_y \sin\theta + I_{yz}\cos\theta)y)}{I_y I_z - I_{yz}^2}\end{aligned} \tag{22}$$

The stress at the neutral axis is zero, so the equation of the neutral axis of *mn* is expressed as below

$$(I_z \cos\theta + I_{yz}\sin\theta)z - (I_y \sin\theta + I_{yz}\cos\theta)y = 0 \tag{23}$$

The angle of φ, which represents the orientation of the neutral axis as shown in Fig. 2, is expressed as below

$$\phi = \arctan\left(\frac{I_y \sin\theta + I_{yz}\cos\theta}{I_z \cos\theta + I_{yz}\sin\theta}\right) \tag{24}$$

2.3 Generalized eccentric compression formula and section core

The rectangular CFST stub column with unequal wall thickness is assumed to be subjected to the eccentric load of *N* with the eccentricity of *e*. When the eccentric load acts in the region of the section core, there is only compressive stress distributing on the cross section. In the elastic stage, the stress of the cross section can be calculated as follows

$$\begin{aligned}\sigma_s &= \frac{(M_y I_z + M_z I_{yz})z - (M_z I_y + M_y I_{yz})y}{I_y I_z - I_{yz}^2} - \frac{N}{BH - (1-m_E)bh} \\ &= N\left(\frac{e((I_z \cos\theta + I_{yz}\sin\theta)z - (I_y \sin\theta + I_{yz}\cos\theta)y)}{I_y I_z - I_{yz}^2} - \frac{1}{BH - (1-m_E)bh}\right) \\ \sigma_c &= m_E\left(\frac{(M_y I_z + M_z I_{yz})z - (M_z I_y + M_y I_{yz})y}{I_y I_z - I_{yz}^2} - \frac{N}{BH - (1-m_E)bh}\right) \\ &= m_E N\left(\frac{e((I_z \cos\theta + I_{yz}\sin\theta)z - (I_y \sin\theta + I_{yz}\cos\theta)y)}{I_y I_z - I_{yz}^2} - \frac{1}{BH - (1-m_E)bh}\right)\end{aligned} \tag{25}$$

Eq. (25) is the generalized eccentric compression formula. The orientation of the neutral axis of *mn* is determined using Eq. (24). The equation of the neutral axis is expressed as below

$$z = \frac{I_y \sin\theta + I_{yz}\cos\theta}{I_z \cos\theta + I_{yz}\sin\theta} y + \frac{I_y I_z - I_{yz}^2}{(BH - (1-m_E)bh)(I_z e\cos\theta + I_{yz} e\sin\theta)} \tag{26}$$

In order to determine the section core, the following four cases are considered:

(1) The eccentric load acts on the critical point (P_1) located on the positive part of the centroidal principal axis of inertia of y'. e_1 represents the distance between C_p and P_1. In this case, the upper left corner of the cross section is the key point, where the stress should be equal to zero. Based on Eq. (25), e_1 is calculated as below

$$e_1 = (I_y I_z - I_{yz}^2) / ((BH - (1-m_E)bh)((I_z \sin\beta - I_{yz}\cos\beta)(\frac{B}{2} + k_p e_z) + (I_y \cos\beta - I_{yz}\sin\beta)(\frac{H}{2} + k_p e_y))) \tag{27}$$

(2) The eccentric load acts on the critical point (P_2) located on the negative part of the y' axis. e_2 represents the distance between C_p and P_2. In this case, the lower right corner of the cross section is the key point, where the stress should be equal to zero. Based on Eq. (25), e_2 is calculated as below

$$e_2 = (I_y I_z - I_{yz}^2) / ((BH - (1-m_E)bh)((I_z \sin\beta - I_{yz}\cos\beta)(\frac{B}{2} - k_p e_z) - (-I_y \cos\beta + I_{yz}\sin\beta)(\frac{H}{2} - k_p e_y))) \tag{28}$$

(3) The eccentric load acts on the critical point (P_3) located on the positive part of the centroidal principal axis of inertia of z'. e_3 represents the distance between C_p and P_3. In this case, the lower left corner of the cross section is the key point, where the stress should be equal to zero. Based on Eq. (25), e_3 is calculated as below

$$e_3 = (I_y I_z - I_{yz}^2) / ((BH - (1-m_E)bh)((I_z \cos\beta + I_{yz}\sin\beta)(\frac{B}{2} + k_p e_z) + (I_y \sin\beta + I_{yz}\cos\beta)(\frac{H}{2} - k_p e_y))) \tag{29}$$

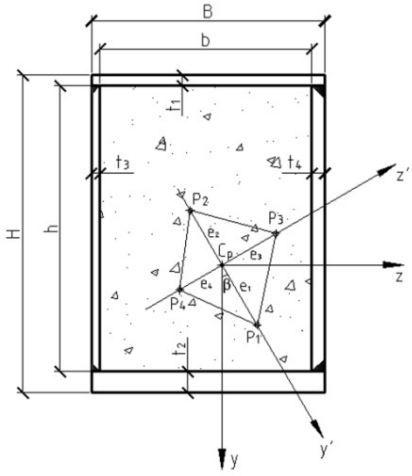

Fig. 4 Section core of rectangular CFST stub columns with unequal wall thickness

(4) The eccentric load acts on the critical point (P_4) located on the negative part of the z' axis. e_4 represents the distance between C_p and P_4. In this case, the upper right corner of the cross section is the key point, where the stress should be equal to zero. Based on Eq. (25), e_4 is calculated as below

$$e_4 = (I_y I_z - I_{yz}^2) / ((BH - (1-m_E)bh)((I_z \cos\beta + I_{yz} \sin\beta)(\frac{B}{2} - k_p e_z) + (I_y \sin\beta + I_{yz} \cos\beta)(\frac{H}{2} + k_p e_y))) \tag{30}$$

The section core is determined by connecting these critical points of P_1, P_2, P_3 and P_4 with straight lines as shown in Fig. 4.

3. Test verification

3.1 Experimental details

The two rectangular CFST stub specimens with unequal wall thickness were tested on a compression testing machine of 2000 kN capacity to verify the formulas. The details of the specimens are shown in Table 1. The compression load was exerted to specimen 1 and specimen 2 on the physical centroid and the geometric centroid respectively. The pace rate of about 0.5 kN/s was fed to the machine. There were 28 strain gauges evenly distributed around the middle cross

Table 1 Details of specimens

Specimen	L (mm)	B (mm)	H (mm)	t_1 (mm)	t_2 (mm)	t_3 (mm)	t_4 (mm)	E_s (GPa)	E_c (GPa)
1	400	110.0	148.3	2.73	9.79	2.73	9.79	206	36.5
2	400	110.3	148.3	2.73	9.79	2.73	9.79	206	36.5

Note: L—Length of the CFST specimen; B—Width of the cross section of the CFST specimen; H— Height of the cross section of the CFST specimen; t_1, t_2, t_3, t_4—Wall thickness of the rectangular steel tube; E_s, E_c—Modulus of elasticity of steel and concrete respectively

(a) Test arrangement of Specimen 1

(b) End of Specimen 1

(c) End of Specimen 2

Fig. 5 Test photos

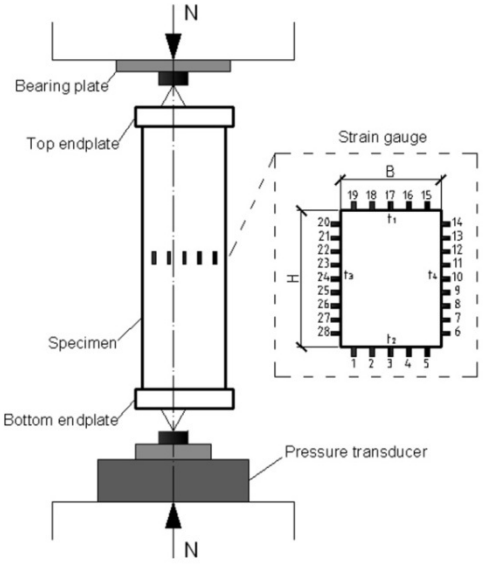

Fig. 6 A schematic view of the test setup

section of each specimen for measuring the longitudinal deformation of the steel tube. The test pictures are shown in Fig. 5. Fig. 6 gives a schematic view of the test arrangements.

3.2 Experimental results and discussions

The test results of specimen 1 are shown in Fig. 7. In the coordinate system shown in Fig. 1, the coordinate of the physical centroid of specimen 1 was obtained as (7.090, 7.090) using Eq. (2). Fig. 7(a) shows all the strain measured by the 28 strain gauges at different load levels. It can be seen from Fig. 7(a) that the whole section deformed uniformly, which proved that the load acted on the physical centroid indeed. The theoretical combined Young's modulus of specimen 1 was calculated as 68.473 GPa using Eq. (4). Fig. 7(b) shows the relationship between the average strain of all the 28 sets of strain, and the average stress obtained through the load divided by the cross-sectional area, which was approximately linear. Through linear regression shown in Fig. 7(b), the experimental combined Young's modulus of specimen 1 was 61.46 GPa, of which the relative error was 10.2%.

The test results of specimen 2 are shown in Fig. 8. In the coordinate system shown in Fig. 2, the coordinate of the geometric centroid of specimen 2 was (-7.097, -7.097). The compression load was exerted to specimen 2 on the geometric centroid, so the orientation angle (θ) of the bending moment was 45.0°. As shown in Fig. 8(a), the orientation angle (β) of the centroidal principal axes of inertia of specimen 2 was -4.4° obtained through Eq. (17). The orientation angle (φ) of the neutral axis (mn) was -30.8° obtained by Eq. (24). The equation of the neutral axis was obtained by Eq. (26) as below

$$z = 187.374 - 0.597y \tag{31}$$

The quantities of e_1, e_2, e_3 and e_4, which determined the section core, were 30.937, 37.335, 24.045 and 32.830 respectively obtained through Eqs. (27)-(30). The section core and the neutral

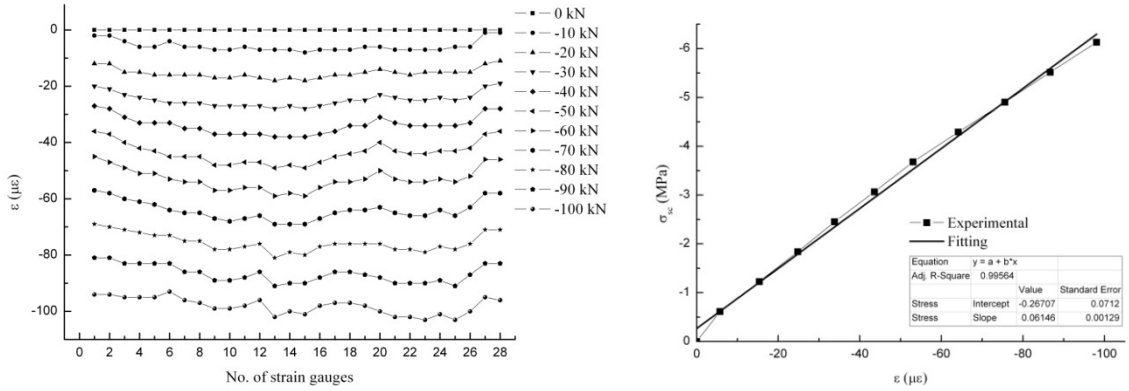

(a) (b)

Fig. 7 Test results of specimen 1 subjected to the compression load on the physical centroid

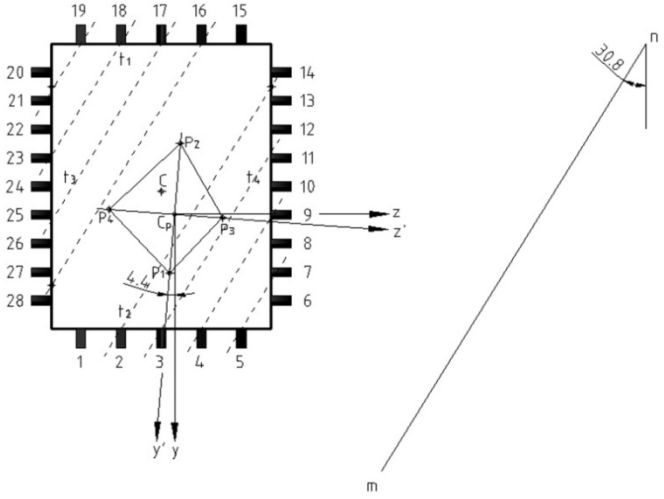

(a)

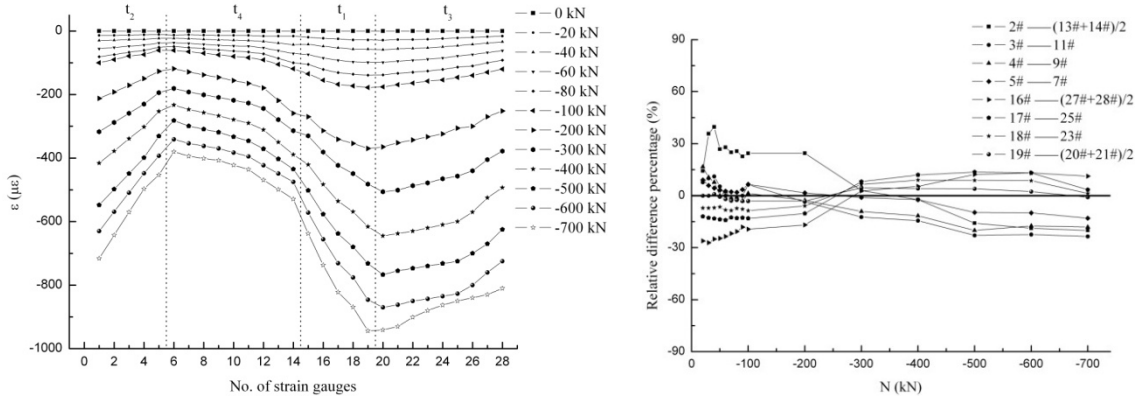

(b) (c)

Fig. 8 Test results of specimen 2 subjected to the compression load on the geometric centroid

axis were illustrated in Fig. 8(a), and the geometric centroid was located within the core. So the full-section compression occurred, which can also be judged from the position of the neutral axis. Fig. 8(b) shows all the strain measured by the 28 strain gauges at different load levels. It can be seen from Fig. 8(b) that all the strain was negative, which indicated the full-section compression and verified the accuracy of the theoretical formulas. From Fig. 8(b), it can be easily found that the strain measured by strain gauge 6 was the minimum and the strain measured by strain gauge 20 was the maximum, which can be proved by the distances between the strain gauges and the neutral axis as shown in Fig. 8(a). Fig. 8(c) shows the comparison of the strain measured by the strain gauges located at the similar distance from the neutral axis. It can be found from Fig. 8(c) that the strain in the similar positions was approximately equal.

4. Conclusions

In this paper, the section properties of the rectangular CFST columns with unequal wall thickness were focused on. The formulas of the physical centroid, the centroidal principal axes of inertia, and the section core were given. In the elastic stage, the generalized bending formula for calculating the stress of the rectangular CFST beams with unequal wall thickness subjected to pure bending, and the generalized eccentric compression formula for calculating the stress of the rectangular CFST stub columns with unequal wall thickness subjected to eccentric compression were derived. The equation of the neutral axis was also given. The two rectangular CFST stub specimens with unequal wall thickness were tested to verify the theoretical formulas.

Acknowledgments

The financial support from the National Natural Science Foundation of China (51278298, 50978162) is gratefully appreciated.

References

Abdalla, S., Abed, F. and Alhamaydeh, M. (2013), "Behavior of CFSTs and CCFSTs under quasi-static axial compression", *J. Constr. Steel Res.*, **90**, 235-244.

Abed, F., Alhamaydeh, M. and Abdalla, S. (2013), "Experimental and numerical investigations of the compressive behavior of concrete filled steel tubes (CFSTs)", *J. Constr. Steel Res.*, **80**, 429-439.

Chen, B., Liu, X. and Li, S.P. (2011), "Performance investigation of square concrete-filled steel tube columns", *J. Wuhan Univ. Technol.*, **26**(4), 730-736.

Chung, K.S., Kim, J.H. and Yoo, J.H. (2013), "Experimental and analytical investigation of high-strength concrete-filled steel tube square columns subjected to flexural loading", *Steel Compos. Struct., Int. J.*, **14**(2), 133-153.

Dai, X. and Lam, D. (2010), "Axial compressive behaviour of stub concrete-filled columns with elliptical stainless steel hollow sections", *Steel Compos. Struct., Int. J.*, **10**(6), 517-539.

Evirgen, B., Tuncan, A. and Taskin, K. (2014), "Structural behavior of concrete filled steel tubular sections (CFT/CFSt) under axial compression", *Thin-Wall. Struct.*, **80**, 46-56.

Giakoumelis, G. and Lam, D. (2004), "Axial capacity of circular concrete-filled tube columns", *J. Constr. Steel Res.*, **60**(7), 1049-1068.

Gupta, P.K., Sarda, S.M. and Kumar, M.S. (2007), "Experimental and computational study of concrete filled steel tubular columns under axial loads", *J. Constr. Steel Res.*, **63**(2), 182-193.

Han, L.H. (2002), "Tests on stub columns of concrete-filled RHS sections", *J. Constr. steel Res.*, **58**(3), 353-372.

Hou, C., Han, L.H. and Zhao, X.L. (2013), "Concrete-filled circular steel tubes subjected to local bearing force: Experiments", *J. Constr. Steel Res.*, **83**, 90-104.

Jiang, Z.W., Li, X.T., Sun, Z.P. and Wang, P.M. (2010), "Preparation and application of self-compacting concrete filled with steel pipe arch", *J. Build. Mater.*, **13**(2), 203-209. [In Chinese]

Kvedaras, A.K., Sauciuvenas, G., Komka, A. and Jarmolajeva, E. (2015), "Analysis of behaviour for hollow/solid concrete-filled CHS steel beams", *Steel Compos. Struct., Int. J.*, **19**(2), 293-308.

Ren, Q.X., Han, L.H., Lam, D. and Hou, C. (2014a), "Experiments on special-shaped CFST stub columns under axial compression", *J. Constr. steel Res.*, **98**, 123-133.

Ren, Q.X., Han, L.H., Lam, D. and Li, W. (2014b), "Tests on elliptical concrete filled steel tubular (CFST) beams and columns", *J. Constr. Steel Res.*, **99**, 149-160.

Uenaka, K. (2014), "Experimental study on concrete filled elliptical/oval steel tubular stub columns under compression", *Thin-Wall. Struct.*, **78**, 131-137.

Xiao, C.Z., Cai, S.H., Chen, T. and Xu, C.L. (2012), "Experimental study on shear capacity of circular concrete filled steel tubes", *Steel Compos. Struct., Int. J.*, **13**(5), 437-449.

CC